J. Fluid Mech. (2006), *vol.* 557, *pp.* 297–306.
doi:10.1017/S0022112006000243 Printed in the United Kingdom

Effect of flexibility on the shear-induced migration of short-chain polymers in parabolic channel flow

By DAVID SAINTILLAN[1], ERIC S. G. SHAQFEH[1,2,3] AND ERIC DARVE[1,3]

[1]Department of Mechanical Engineering, Stanford University, Stanford, CA 94305, USA
[2]Department of Chemical Engineering, Stanford University, Stanford, CA 94305, USA
[3]Institute for Computational and Mathematical Engineering, Stanford University, Stanford, CA 94305, USA

(Received 18 December 2005 and in revised form 1 April 2006)

We use Brownian dynamics to investigate the effect of chain flexibility on the cross-streamline migration of short polymers in a pressure-driven flow between two infinite flat plates. A simulation method is described that models a polymer molecule at the Kuhn step level as a chain of N freely jointed Brownian rods, and includes multibody hydrodynamic interactions between the chain segments and the surrounding channel walls. Our study confirms the existence of shear-induced migration away from the solid boundaries toward the channel centreline as a result of wall hydrodynamic interactions. At a fixed ratio H/R_g of the channel width to the bulk radius of gyration, and at a fixed value of the Weissenberg number Wi, simulations show that migration is not significantly influenced by flexibility for chains of length $N \geqslant 2$. Much weaker migration is observed however for fully rigid chains ($N = 1$), and a mechanism is discussed to explain migration in that case.

1. Introduction

The recent advent of microfluidics as a tool for the miniaturization of chemical and biological assays has spurred a renewed interest in the behaviour of macromolecules and colloids in confinement. Interactions with boundaries and the short-scale variations of fluid flows in such environments indeed result in unusual dynamics (e.g. Jendrejack *et al.* 2003; Chen *et al.* 2005), many aspects of which remain poorly understood. One phenomenon of interest, addressed in this paper, is the cross-streamline migration of polymeric molecules in inhomogeneous flows, which has implications for the effective rheology and transport of flowing polymer solutions. Numerous studies have addressed this problem in the past (see the review by Agarwal, Dutta & Mashelkar 1994), yet often disagree on issues as fundamental as the direction of migration. A wide variety of physical mechanisms, such as wall exclusion, configuration-dependent diffusivities or hydrodynamic interactions, may contribute to the phenomenon, thereby making general predictions difficult to formulate.

The case of long-chain flexible polymers such as DNA molecules has received much attention recently, both in experiments (Chen *et al.* 2005; Fang, Hu & Larson 2005) and computer simulations (Jendrejack *et al.* 2003, 2004; Chen *et al.* 2005; Usta, Ladd & Butler 2005). The consensus from these studies is that flexible polymers in

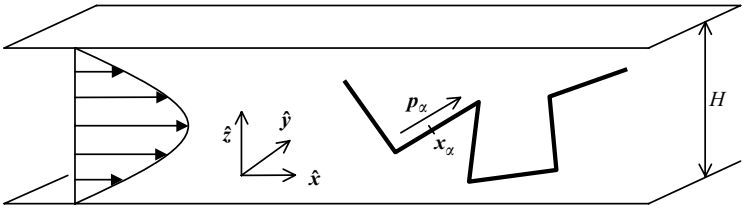

FIGURE 1. Problem geometry: we consider the pressure-driven flow of a dilute polymer solution between two infinite flat plates. A polymer molecule is modelled as a chain of freely jointed hydrodynamically interacting Brownian rods.

a pressure-driven channel flow migrate away from the walls toward the centreline, leading to the formation of a depletion layer, whose characteristic thickness greatly exceeds the radius of gyration of a single molecule. Graham and coworkers proposed a theoretical model explaining the migration as a consequence of hydrodynamic interactions between the walls and the entropic force dipole exerted by a stretched polymer on the fluid, leading to a deterministic drift away from the walls (Jendrejack *et al.* 2004; Ma & Graham 2005). As higher shear rates result in stronger molecular stretching, the drift is expected to increase with flow strength, as is indeed observed experimentally (Fang *et al.* 2005) and in numerical simulations (Jendrejack *et al.* 2004).

Experimental evidence of depletion layers in flowing solutions of rigid and semi-flexible polymers has also been reported (Ausserré *et al.* 1991). Yet in these systems the depletion layer thickness, which also increases with shear rate, typically remains of the order of the radius of gyration of a molecule. Models for rigid polymers have focused on steric exclusion with the walls (Ausserré *et al.* 1991; de Pablo, Öttinger & Rabin 1992; Schiek & Shaqfeh 1997). While neglecting wall hydrodynamic interactions, these studies were reasonably successful at explaining experimental observations, including the thickening of the depletion layer in strong flows, which may be a consequence of more frequent collisions with the walls owing to an increased rate of molecular tumbling.

The precise effects of wall hydrodynamic interactions and the applicability of the entropic dipole model of Ma & Graham (2005) to the case of less flexible polymers therefore deserve closer attention. In this paper we employ Brownian dynamics simulations to address these issues. A Kuhn-step-level polymer model is described in § 2, allowing the simulation of a short chain of a few persistence lengths that includes multibody hydrodynamic interactions between the chain segments and the channel walls. Results are discussed in § 3, where we emphasize the effect of flexibility. A summary and concluding remarks are given in § 4.

2. Model and numerical implementation

We consider the pressure-driven flow of a dilute polymer solution between two infinite flat plates separated by a distance H (figure 1). A polymer molecule is modelled as a chain composed of N freely jointed rigid rods (Kuhn steps) of length L and aspect ratio A, as previously done by Nyland *et al.* (1996), Ådland & Mikkelsen (2004), and most recently Butler & Shaqfeh (2005). The spatial configuration of a given rod α is determined by the position $\boldsymbol{x}_\alpha$ of its centre of mass and by a unit vector $\boldsymbol{p}_\alpha$ aligned with its major axis. The motion of each rod is described using slender-body theory for Stokes flow, which relates the linear and angular velocities

of the rod to the fluid velocity $\boldsymbol{u}(\boldsymbol{x})$ and to a line distribution $\boldsymbol{f}_\alpha$ of point force singularities along the rod axis (Batchelor 1970):

$$\dot{\boldsymbol{x}}_\alpha + s_\alpha \dot{\boldsymbol{p}}_\alpha - \boldsymbol{u}(\boldsymbol{x}_\alpha + s_\alpha \boldsymbol{p}_\alpha) = (\boldsymbol{I} + \boldsymbol{p}_\alpha \boldsymbol{p}_\alpha) \cdot \boldsymbol{f}_\alpha(s_\alpha), \tag{2.1}$$

where s_α denotes a linear coordinate along the axis of the rod of interest, with origin the centre of the rod. Equation (2.1), in which terms of order $(\log 2A)^{-1}$ have been neglected, is an asymptotic approximation valid for high aspect ratios ($A \gg 1$). In the present discussion lengths and times are made dimensionless using the characteristic scales $l_c = L$ and $t_c = 4\pi\mu L^3/kT \log 2A$, where μ and kT are the viscosity and thermal energy of the solvent, respectively. The linear and angular velocities of the rod are obtained by integration of equation (2.1):

$$\dot{\boldsymbol{x}}_\alpha = \int_{-1/2}^{1/2} \boldsymbol{u}(\boldsymbol{x}_\alpha + s_\alpha \boldsymbol{p}_\alpha)\, \mathrm{d}s_\alpha + (\boldsymbol{I} + \boldsymbol{p}_\alpha \boldsymbol{p}_\alpha) \cdot \boldsymbol{F}_\alpha, \tag{2.2}$$

$$\dot{\boldsymbol{p}}_\alpha = 12(\boldsymbol{I} - \boldsymbol{p}_\alpha \boldsymbol{p}_\alpha) \cdot \int_{-1/2}^{1/2} s_\alpha \boldsymbol{u}(\boldsymbol{x}_\alpha + s_\alpha \boldsymbol{p}_\alpha)\, \mathrm{d}s_\alpha + 12(\boldsymbol{I} - \boldsymbol{p}_\alpha \boldsymbol{p}_\alpha) \cdot \tilde{\boldsymbol{F}}_\alpha, \tag{2.3}$$

where $\boldsymbol{F}_\alpha$ and $\tilde{\boldsymbol{F}}_\alpha$ denote the zeroth and first moments of the force distribution along the rod axis, and are related to the total external force and torque on the rod.

Hydrodynamic interactions between rods and with the walls are captured through the fluid velocity $\boldsymbol{u}$ in equations (2.1)–(2.3), which is the sum of the imposed pressure-driven flow $\boldsymbol{u}_\infty$ and the disturbance velocities induced by the other rods in the polymer chain, and by the presence of the walls. For example, along rod α, $\boldsymbol{u}$ becomes

$$\boldsymbol{u}(\boldsymbol{x}) = \boldsymbol{u}_\infty(\boldsymbol{x}) + \frac{1}{2\log 2A} \sum_{\beta=1}^{N} \int_{-1/2}^{1/2} \boldsymbol{G}^W(\boldsymbol{x}; \boldsymbol{x}_\beta + s_\beta \boldsymbol{p}_\beta) \cdot \boldsymbol{f}_\beta(s_\beta)\, \mathrm{d}s_\beta, \tag{2.4}$$

where $\boldsymbol{G}^W(\boldsymbol{x}; \boldsymbol{x}_0)$ denotes the Green's function for Stokes flow in the geometry of interest, from which the Oseen–Burgers tensor is subtracted when $\beta = \alpha$. In this work the exact Green's function between two infinite flat plates (Liron & Mochon 1976) was implemented in its regularized form as described by Staben, Zinchenko & Davis (2003). In the case of a pressure-driven flow between two flat plates, the imposed fluid velocity is

$$\boldsymbol{u}_\infty(\boldsymbol{x}) = Pe\, \frac{z}{L}\left(1 - \frac{z}{H}\right)\hat{\boldsymbol{x}}, \quad \text{where} \quad Pe = \gamma_w\, t_c. \tag{2.5}$$

The Péclet number Pe, which measures the relative effects of the imposed flow and of thermal diffusion on the dynamics of a chain segment, is defined as the product of the wall shear rate $\gamma_w = 6U_0/H$ (where U_0 is the cross-sectional average fluid velocity) and the characteristic thermal time scale t_c defined above.

Equations (2.1)–(2.4) constitute an integral system for the force distributions along the chain segments. While this system can in principle be solved numerically using quadrature, we describe a different approach allowing a more efficient, albeit approximate, solution. Following Butler & Shaqfeh (2005), we expand the force distribution in Legendre polynomials and only retain the first two terms:

$$\boldsymbol{f}_\alpha(s_\alpha) \approx \boldsymbol{F}_\alpha + 12 s_\alpha [(\boldsymbol{I} - \boldsymbol{p}_\alpha \boldsymbol{p}_\alpha) \cdot \tilde{\boldsymbol{F}}_\alpha + \mathscr{S}_\alpha \boldsymbol{p}_\alpha]. \tag{2.6}$$

We have introduced the stresslet $\mathscr{S}_\alpha$ on rod α, which is a scalar quantity arising from the inability of the rod to stretch or compress along its major axis:

$$\mathscr{S}_\alpha = -\frac{1}{2}\int_{-1/2}^{1/2} s_\alpha \boldsymbol{p}_\alpha \cdot \boldsymbol{u}(\boldsymbol{x}_\alpha + s_\alpha \boldsymbol{p}_\alpha)\,\mathrm{d}s_\alpha. \tag{2.7}$$

The linearization (2.6) reduces the integral system for the force distributions to an $N \times N$ linear system for the stresslets on the chain segments, which is easily inverted by Gaussian elimination. Once the stresslets are known they can be substituted into the linearized force distribution (2.6), which itself is used to obtain the disturbance velocity (2.4). The rod motions are then inferred using equations (2.2)–(2.3). The method thus described allows the calculation of the rod velocities in terms of the imposed flow velocity and of the external force and torque on each rod, which can be written symbolically as

$$\dot{\mathscr{R}} = \dot{\mathscr{R}}_\infty + \mathscr{M}(\mathscr{R}) \cdot \mathscr{F}, \tag{2.8}$$

where $\mathscr{R}$ denotes a generalized position vector containing the centre-of-mass positions and orientations of all the rods, and $\mathscr{F}$ is a generalized force vector containing the external force and first force moment on each rod. The tensor $\mathscr{M}$ is the grand mobility operator, which accounts for hydrodynamic interactions between rods and with the walls up to the stresslet term.

In this work the rods are subjected to constraint forces, excluded-volume forces, and Brownian forces, all of which are discussed in detail by Butler & Shaqfeh (2005). The constraint forces $\mathscr{F}^c$ are required to maintain the integrity of the chain, and are calculated using the method of Lagrange multipliers to satisfy the constraint that adjacent chain segments must remain linked. Excluded-volume interactions are captured through strong and short-ranged repulsive forces $\mathscr{F}^e$, which prevent overlap between chain segments and with the channel walls. Finally the Brownian forces $\mathscr{F}^b$ model collisions between the solvent molecules and the chain, and are stochastic variables that must satisfy the fluctuation–dissipation theorem of statistical mechanics (Doi & Edwards 1986):

$$\langle \mathscr{F}^b(t) \rangle = 0, \quad \langle \mathscr{F}^b(t)\mathscr{F}^b(t') \rangle = 2\delta(t-t')\mathscr{M}^{-1}, \tag{2.9}$$

where $\langle\cdot\rangle$ denotes the ensemble average, and $\delta(t)$ is the Dirac delta function. They are calculated in a classic manner as

$$\mathscr{F}^b = \sqrt{\frac{2}{\Delta t}}\mathscr{B} \cdot \mathscr{W}, \tag{2.10}$$

where Δt is the time step, $\mathscr{B}$ satisfies $\mathscr{B} \cdot \mathscr{B}^T = \mathscr{M}^{-1}$ and is obtained by Cholesky decomposition of the inverse of the grand mobility matrix, and $\mathscr{W}$ is a vector of length $6N$ containing random numbers from a Gaussian distribution with zero mean and unit variance. Finally, the stochastic motion of the chain inside the gap is integrated in time using Fixman's midpoint algorithm (Fixman 1978), which is appropriate for Brownian systems with configuration-dependent diffusivities (Grassia, Hinch & Nitsche 1995).

3. Results and discussion

In the following discussion, flow strengths are expressed in terms of the Weissenberg number Wi, or ratio of the longest bulk relaxation time λ of the chain to the characteristic time scale of the flow (defined as the inverse of the wall shear rate):

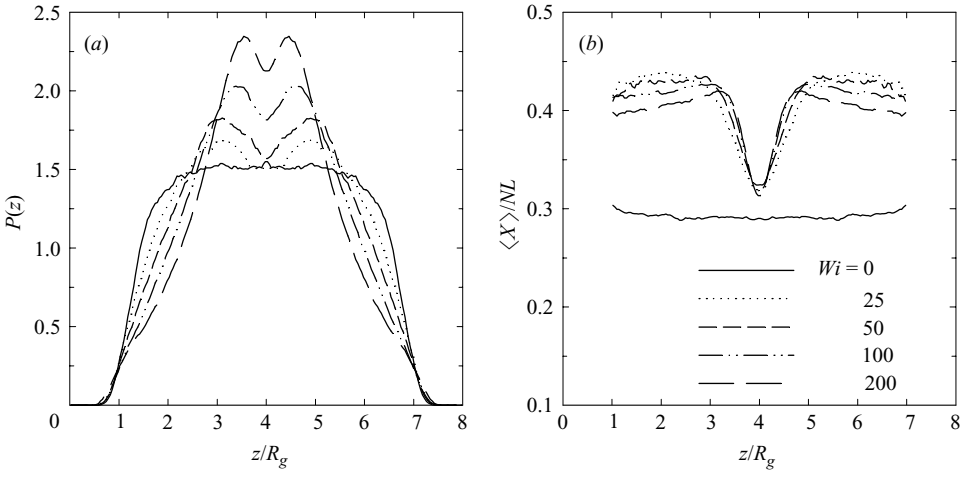

FIGURE 2. (*a*) Centre-of-mass concentration profile and (*b*) average normalized stretch in the flow direction in a channel of width $H = 8R_g$ at various flow strengths, for a molecule composed of $N = 6$ segments of aspect ratio $A = 10$.

$Wi = \lambda/\gamma_w^{-1}$. Equivalently, the Weissenberg number is given by the product of the Péclet number and the dimensionless chain relaxation time. As we shall see, lengths are also conveniently expressed in terms of the bulk radius of gyration R_g.

Typical concentration profiles across the gap are shown in figure 2(*a*) for a chain composed of $N = 6$ segments and for various flow strengths in a channel of width $H = 8R_g$. The profiles, which are qualitatively similar to those obtained previously by other authors in the case of much longer chains (Jendrejack *et al.* 2003, 2004; Usta *et al.* 2005), present several interesting features. A clear depletion layer is observed in the vicinity of the walls. While this depletion layer exists even in the absence of flow ($Wi = 0$), where its thickness is of the order of one radius of gyration, it is shown to grow as Wi increases, resulting in fairly peaked distributions in strong flows. The profiles for $Wi > 0$ also exhibit a slight depletion at the centreline, which is a consequence of the gradient in the cross-streamline centre-of-mass diffusivity resulting from the non-uniform stretching of the chain in the inhomogeneous shear. This non-uniform stretching is illustrated in figure 2(*b*), showing the average molecular stretch $\langle X \rangle$ in the flow direction, normalized by the chain contour length NL. While the stretch profile is uniform in the absence of flow, significant variations of $\langle X \rangle$ across the gap are visible when flow is applied, with markedly stronger molecular stretch near the walls than near the centreline owing to the variations in shear rate. Interestingly, the dependence of $\langle X \rangle$ on the flow strength is rather weak when $Wi > 0$, a possible consequence of hydrodynamic interaction with the walls as further discussed below.

To confirm the role of hydrodynamic interactions (HI) in the migration of the chains toward the centreline, simulations were performed in which the interactions were completely turned off, corresponding to a freely draining chain with anisotropic drag. The results are summarized in figure 3, showing concentration profiles and average stretch profiles with and without HI. The figure also shows profiles with a different level of modelling, in which the stresslet on each rod (equation (2.7)) was calculated based on $\boldsymbol{u}_\infty$ only: in that case each segment feels the disturbance velocity induced by the other segments placed in the imposed field $\boldsymbol{u}_\infty$ (including the associated wall disturbance), but the multiple reflections between the segments are not included (two-body HI).

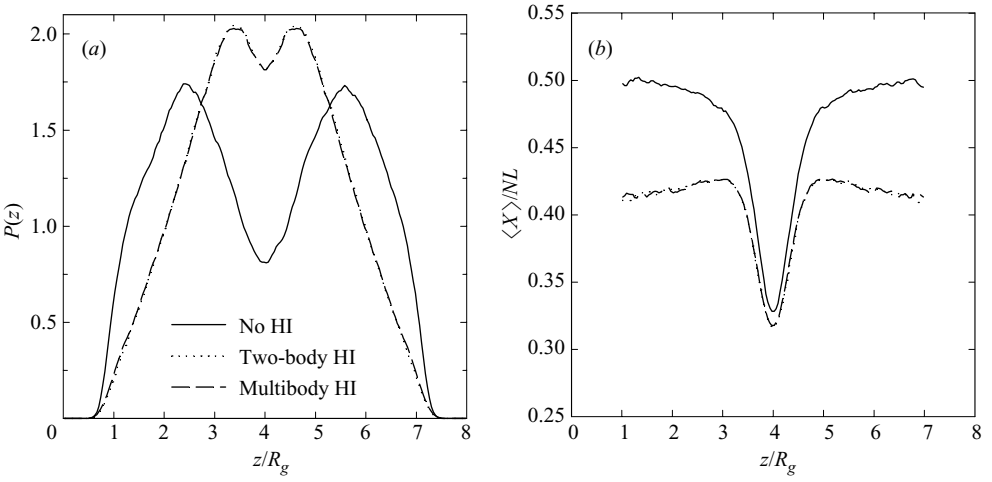

FIGURE 3. Influence of hydrodynamic interactions on (*a*) the centre-of-mass concentration profile and (*b*) the average normalized stretch for a molecule composed of $N = 6$ segments of aspect ratio $A = 10$, in a channel of width $H = 8R_g$ at $Wi = 100$. The different curves show different levels of modelling: no hydrodynamic interactions, two-body hydrodynamic interactions, and multibody hydrodynamic interactions at the stresslet level.

While the profiles corresponding to the two levels of modelling for HI cannot be distinguished, completely neglecting hydrodynamic interactions yields qualitatively different results, with a very strong depletion at the channel centreline and no clear migration away from the walls (other than that due to excluded volume): in that case the depletion at the centreline is a consequence of the anisotropic drag on the chain segments, which results in a gradient in cross-streamline diffusivity qualitatively similar to that observed for a single Brownian rod (Nitsche & Hinch 1997; Schiek & Shaqfeh 1997). This is in qualitative agreement with the previous observations of Jendrejack *et al.* (2004) for bead–spring chains, and confirms the importance of wall hydrodynamic interactions in the description of channel flows of flexible molecules. The effects of HI on molecular stretch are also visible in figure 3(*b*), where it appears that hydrodynamic interactions reduce the ability of the chain to stretch in the vicinity of the walls. Note that this effect has also been observed in experiments (Fang *et al.* 2005), and may explain the weak dependence of molecular stretch on flow strength observed in figure 2(*b*).

Figure 4 illustrates the influence of chain flexiblity (measured by the number of Kuhn steps N) on the cross-streamline migration. In figure 4(*a*) the Péclet number Pe and the ratio H/L of the channel width to the Kuhn step length are held constant: in this situation longer chains migrate much more strongly away from the walls than shorter ones, as exemplified by the very flat and very peaked profiles for $N = 1$ and $N = 10$ respectively. In this sense chain flexibility appears to facilitate migration, a consequence of the entropic force dipole exerted on the fluid (Ma & Graham 2005), which is stronger in longer chains but non-existent in the limit of a fully rigid rod ($N = 1$), where the only force dipole on the fluid is deterministic and due to the stresslet induced by the imposed shear rate. Most interestingly, the concentration profiles for the chain lengths $N \geqslant 2$ are observed to collapse onto a single curve when the Weissenberg number Wi and the ratio H/R_g of the channel width to the bulk radius of gyration are held constant, as shown in figure 4(*b*) for $Wi = 50$ and $H = 8R_g$. Note that a similar collapse is also observed at other values of the

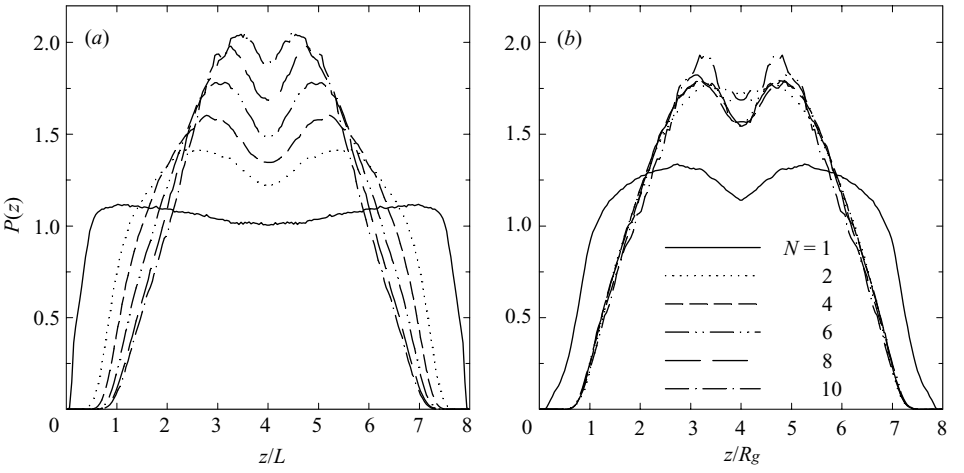

FIGURE 4. Concentration profiles for various chain lengths N when: (a) the Péclet number Pe and ratio H/L of the channel width to the Kuhn step length are held constant ($Pe = 100$, $H/L = 8$); (b) the Weissenberg number Wi and ratio H/R_g of the channel width to the bulk radius of gyration are held constant ($Wi = 50$, $H/R_g = 8$).

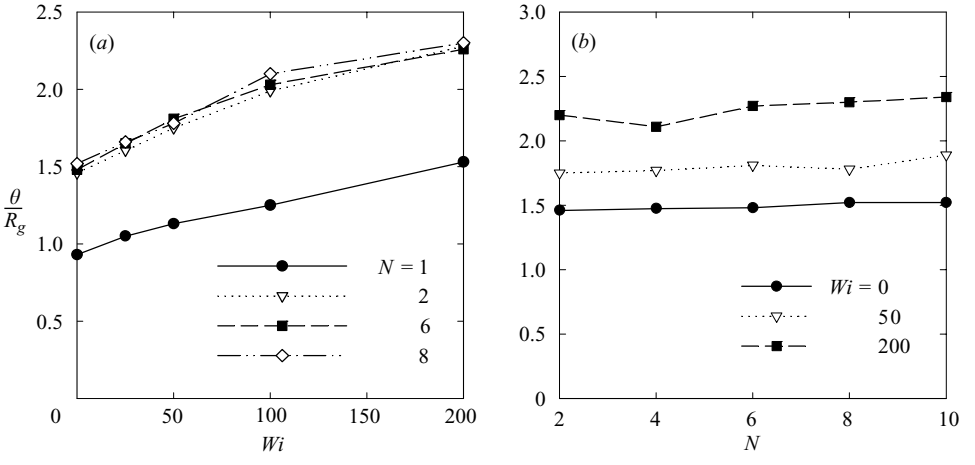

FIGURE 5. Depletion layer thickness θ (measured as the distance from the wall where the concentration reaches its mean value) as a function of: (a) the flow strength (or Weissenberg number Wi), and (b) the chain length N, for molecules composed of N segments of aspect ratio $A = 10$ in a channel of width $H = 8R_g$.

Weissenberg number. This suggests in particular that Wi and H/R_g, rather than Pe and H/L, are the appropriate dimensionless groups for quantifying the effects of flow strength and channel width on the shear-induced migration. The fully rigid case ($N = 1$) differs qualitatively however, as shown in figure 4(b): it is characterized by a much weaker migration (the mechanism for which is discussed below), and by a fairly strong depletion at the centreline as a result of the gradient in centre-of-mass diffusivity induced by the differential alignment of the rod across the channel width (Nitsche & Hinch 1997; Schiek & Shaqfeh 1997).

Some of the observations mentioned above are summarized in figure 5, showing the effects of flow strength and chain flexiblity on the thickness θ of the wall depletion

layer, defined as the position away from the walls where the concentration profile reaches its mean value. Figure 5(*a*) illustrates the thickening of the depletion layer with flow strength: θ/R_g is observed to increase from a value of approximately 1.5 in the absence of flow ($Wi=0$) up to approximately 2.3 at $Wi=200$ (for flexible chains $N\geqslant 2$). Again when θ is scaled by R_g the dependence on chain length is negligible, as the depletion layer thicknesses for $N=2$, 6, and 8 collapse onto a single master curve. The insensitivity of the depletion layer thickness to chain length is also illustrated in figure 5(*b*), where it is observed that for a given flow strength θ/R_g does not depend on N over the range $N=2$ to 10. Figure 5(*a*) also confirms the significantly different behaviour of fully rigid chains ($N=1$), for which depletions layers are much thinner than for flexible chains; yet a thickening of θ/R_g with flow strength is also observed.

The case of a fully rigid polymer ($N=1$) was shown to differ qualitatively from the flexible case and therefore deserves further attention. Unlike a flexible chain which relaxes by entropic recoil, a rodlike polymer relaxes by randomization of its orientation. The mechanism for shear-induced migration proposed by Jendrejack *et al.* (2004) and Ma & Graham (2005) for flexible polymers, based on the entropic force dipole exerted by a chain on the fluid as it tries to recoil while being stretched by flow, therefore does not trivially carry over to rodlike polymers. Owing to its resistance to stretching, a rigid rod in a non-uniform flow also exerts a force dipole on the fluid, the magnitude of which is the stresslet $\mathscr{S}$ defined in equation (2.7). While $\mathscr{S}$ clearly scales with flow strength, its sign and magnitude both depend on the orientation of the rod relative to the imposed flow, which itself is determined by the balance between fluid flow and thermal diffusion: its interaction with the nearby boundaries is unclear *a priori*.

These considerations can be made more quantitative using similar arguments as in Ma & Graham (2005). The force dipole $\boldsymbol{D}$ on a freely suspended rod with orientation $\boldsymbol{p}$ in the pressure-driven flow equation (2.5) is given in dimensionless variables by

$$\boldsymbol{D}=\mathscr{S}\left(\boldsymbol{pp}-\frac{\boldsymbol{I}}{3}\right)\approx\frac{1}{24}p_x p_z\gamma(z)\left(\boldsymbol{pp}-\frac{\boldsymbol{I}}{3}\right), \tag{3.1}$$

where $\mathscr{S}$ is the stresslet on the rod, and $\gamma(z)=\partial u_\infty/\partial z=Pe(1-2z/H)/L$ is the local shear rate. The rightmost expression in equation (3.1) is the leading-order term in an expansion of equation (2.7). As shown by Smart & Leighton (1991), a force dipole $\boldsymbol{D}$ in the vicinity of a no-slip wall is subject to a drift velocity as a result of hydrodynamic interactions:

$$\boldsymbol{U}^D=-\frac{3}{8h^2\log 2A}\left(\boldsymbol{I}+\frac{1}{2}\boldsymbol{nn}\right)\cdot\boldsymbol{D}\cdot\boldsymbol{n}, \tag{3.2}$$

where $\boldsymbol{n}$ is a unit vector normal to the plane of the wall and h is the distance from the wall. Substituting (3.1) into (3.2), and superimposing the effects of both walls (an approximation valid for large gaps $H/L\gg 1$), we find that the cross-streamline drift velocity of the rigid rod is to leading order

$$U_z^D=-\frac{\gamma(z)}{128\log 2A}f(\phi)\left[\frac{1}{z^2}-\frac{1}{(H-z)^2}\right], \tag{3.3}$$

where $f(\phi)$ is a function of the projected angle ϕ of the rod orientation vector $\boldsymbol{p}$ onto the (x,z)-plane and measured with respect to the x-axis: $f(\phi)=\cos\phi\sin\phi(3\sin^2\phi-1)$. Note that a more accurate albeit less intuitive expression for U_z^D accounting for multipole reflections between the rod and the two walls is easily derived using the slender-body theory described in § 2.

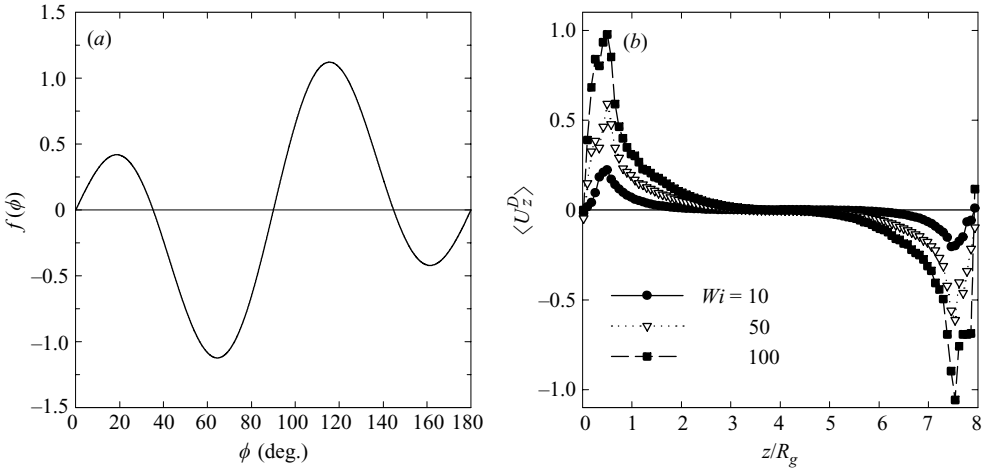

FIGURE 6. (*a*) Dependence $f(\phi)$ of the cross-streamline drift velocity U_z^D upon the projected angle ϕ of a rigid rod in the (x, z)-plane: $f(\phi) = \cos\phi \sin\phi(3\sin^2\phi - 1)$. (*b*) Profile of the mean cross-streamline drift velocity $\langle U_z^D \rangle$ for a rod of aspect ratio $A = 10$ in a channel of width $H = 8R_g$, at various flow strengths, obtained from simulations.

Equation (3.3) shows that the rod can migrate either toward or away from the walls depending on the sign of $f(\phi)$, which is plotted on figure 6(*a*). We see that both signs are possible depending on the value of the projected angle. In a sufficiently strong shear flow a rod will spend most of its time almost aligned in the flow direction ($\phi \gtrsim 0$), leading to a migration away from the walls ($f(\phi) \geqslant 0$ for $0 \leqslant \phi \leqslant 35°$). Note however that $f(0) = 0$, so that a very strong flow, while leading to large values of the shear rate $\gamma(z)$ in equation (3.3) for U_z^D, will also result in a very strong alignment of the rod for which $\langle f(\phi) \rangle$ may be small: the overall effect on the migration is therefore a subtle combination of the magnitude of the dipole induced on the rod and the orientation of the rod with respect to the flow. The precise effect of flow strength is illustrated in figure 6(*b*), showing the mean cross-streamline drift velocity $\langle U_z^D \rangle$ as a function of position and for various values of the Weissenberg number, obtained using the full slender-body theory of § 2 and calculated numerically over the course of the simulations. In particular, migration away from the walls is observed, and the magnitude of the drift increases with flow strength. Figure 6(*b*) also shows that the drift velocity is quite weak in the bulk of the channel, which may explain the relatively weak migration observed in figure 4.

4. Concluding remarks

We have performed Brownian dynamics simulations of short-chain polymers in the pressure-driven flow between two infinite flat plates, in which we modelled a polymer molecule as a chain of freely jointed hydrodynamically interacting Brownian rods. Our simulations showed that cross-streamline migration toward the channel centreline occurs as a result of hydrodynamic interaction of the polymer with the wall. While flexible chains of various lengths ($2 \leqslant N \leqslant 10$) all behave in a similar fashion for given values of the Weissenberg number Wi and of H/R_g, the ratio of the channel width to the bulk radius of gyration, fully rigid polymers ($N = 1$) are observed to undergo a much weaker migration, the mechanism for which differs qualitatively and is based on

a coupling between the stresslet induced by the flow on the rod, the orientation of the rod as determined by the balance of flow and thermal fluctuations, and hydrodynamic interactions with the walls.

The authors gratefully acknowledge funding from Canon (E.D.) and from a Gerald J. Lieberman Graduate Fellowship (D.S.).

REFERENCES

Ådland, H. M. & Mikkelsen, A. 2004 Brownian dynamics simulations of needle chains and nugget chain polymer models – rigid contraint conditions versus infinitely stiff springs. *J. Chem. Phys.* **120**, 9848–9858.

Agarwal, U. S., Dutta, A. & Mashelkar, R. A. 1994 Migration of macromolecules under flow: the physical origin and engineering implications. *Chem. Engng Sci.* **11**, 1693–1717.

Ausserré, D., Edwards, J., Lecourtier, J., Hervet, H. & Rondelez, F. 1991 Hydrodynamic thickening of depletion layers in colloidal solutions. *Europhys. Lett.* **14**, 33–38.

Batchelor, G. K. 1970 Slender-body theory for particles of arbitrary cross-section in Stokes flow. *J. Fluid Mech.* **44**, 419–440.

Butler, J. E. & Shaqfeh, E. S. G. 2005 Brownian dynamics simulations of a flexible polymer chain which includes continuous resistance and multibody hydrodynamic interactions. *J. Chem. Phys.* **122**, 014901.

Chen, Y.-L., Graham, M. D., de Pablo, J. J., Randall, G. C., Gupta, M. & Doyle, P. S. 2005 Conformation and dynamics of single DNA molecules in parallel-plate slit geometry. *Phys. Rev.* E **70**, 060901.

De Pablo, J. J., Öttinger, H. C. & Rabin, Y. 1992 Hydrodynamic changes of the depletion layer of dilute polymer solutions near a wall. *AIChE J.* **38**, 273–283.

Doi, M. & Edwards, S. F. 1986 *The Theory of Polymer Dynamics*. Oxford University Press.

Fang, L., Hu, H. & Larson, R. G. 2005 DNA configurations and concentration in shearing flow near a glass surface in a microchannel. *J. Rheol.* **127**, 127–138.

Fixman, M. 1978 Simulation of polymer dynamics. I. General theory. *J. Chem. Phys.* **69**, 1527–1537.

Grassia, P. S., Hinch, E. J. & Nitsche, L. C. 1995 Computer simulations of Brownian motion of complex systems. *J. Fluid Mech.* **282**, 373–403.

Jendrejack, R. M., Dimalanta, E. T., Schwartz, D. C., Graham, M. D. & de Pablo, J. J. 2003 DNA dynamics in a microchannel. *Phys. Rev. Lett.* **91**, 038102.

Jendrejack, R. M., Schwartz, D. C., de Pablo, J. J. & Graham, M. D. 2004 Shear-induced migration in flowing polymer solutions: Simulation of long-chain DNA in microchannels. *J. Chem. Phys.* **120**, 2513–2529.

Liron, N. & Mochon, S. 1976 Stokes flow for a Stokeslet between two parallel flat plates. *J. Engng Maths* **10**, 287–303.

Ma, H. & Graham, M. D. 2005 Theory of shear-induced migration in dilute polymer solutions near solid boundaries. *Phys. Fluids* **17**, 083103.

Nitsche, L. C. & Hinch, E. J. 1997 Shear-induced lateral migration of Brownian rigid rods in parabolic channel flow. *J. Fluid Mech.* **332**, 1–21.

Nyland, G. H., Skjetne, P., Mikkelsen, A. & Elgsaeter, A. 1996 Brownian dynamics simulation of needle chains. *J. Chem. Phys.* **105**, 1198–1207.

Schiek, R. L. & Shaqfeh, E. S. G. 1997 Cross-streamline migration of slender Brownian fibres in plane Poiseuille flow. *J. Fluid Mech.* **332**, 23–39.

Smart, J. R. & Leighton, D. T. 1991 Measurement of the drift of a droplet due to the presence of a plane. *Phys. Fluids* A **3**, 21–28.

Staben, M. E., Zinchenko, A. Z. & Davis, R. H. 2003 Motion of a particle between two parallel plane walls in low-Reynolds-number Poiseuille flow. *Phys. Fluids* **15**, 1711–1733.

Usta, O. B., Ladd, A. J. C. & Butler, J. E. 2005 Lattice-Boltzmann simulations of the dynamics of polymer solutions in periodic and confined geometries. *J. Chem. Phys.* **122**, 094902.